Ressortforschungsberichte zum Strahlenschutz

Untersuchung des Risikos für kardiovaskuläre Erkrankungen nach einer Strahlenexposition mit niedrigen Dosen an Biopsieproben von Majak-Arbeitern - Vorhaben 3617S32261

Auftragnehmer:
Helmholtz Zentrum München

O. Azimzadeh
T. Azizova
S. Tapio

Das Vorhaben wurde mit Mitteln des Bundesministeriums für Umwelt, Naturschutz und nukleare Sicherheit (BMU) und im Auftrag des Bundesamtes für Strahlenschutz (BfS) durchgeführt.

Bundesamt für Strahlenschutz

BfS-RESFOR-152/19

Bitte beziehen Sie sich beim Zitieren dieses Dokumentes immer auf folgende URN:
urn:nbn:de:0221-2019091719217

Salzgitter, September 2019

Analysis of risks of cardiovascular diseases after radiation exposure at low doses in heart samples from Mayak nuclear workers (3617S32261)

Untersuchung des Risikos für kardiovaskuläre Erkrankungen nach einer Strahlenexposition mit niedrigen Dosen an Biopsieproben von Majak-Arbeitern (3617S32261)

O. Azimzadeh, T. Azizova , S. Tapio

TABLE OF CONTENTS

Untersuchung des Risikos für kardiovaskuläre Erkrankungen nach einer Strahlenexposition mit niedrigen Dosen an Biopsieproben von Majak-Arbeitern (3617S32261)

ZUSAMMENFASSUNG

Epidemiologische Studien zeigen einen signifikanten Anstieg der ischämischen Herzkrankheiten (IHK) bei den Arbeitern der Plutoniumanreicherungsanlage Majak in der Russischen Föderation, die mit der Höhe ihrer externen Gesamtgammastrahlendosis in Zusammenhang gebracht werden kann. Unsere bisherigen Studien mit Maus- und Humanherzproben deuten darauf hin, dass Herzschäden nach hohen Dosen ionisierender Strahlung mit einer anhaltenden Veränderung des Herzstoffwechsels durch die Hemmung des Peroxisom-Proliferator-aktivierten Rezeptors (PPAR) alpha einhergehen. Das Ziel der vorliegenden Studie war es, diese Ergebnisse mit Hilfe eines zellulären Modells (Kardiomyozyten) sowie mit zusätzlichen Herzproben aus den Autopsien von weiteren Majak-Arbeitern zu validieren.

Kardiomyozyten wurden kultiviert, mit Dosen von 0 Gy und 2 Gy bestrahlt (was ungefähr der Strahlendosis der Kontroll- und Hochdosisgruppe der menschlichen Gewebeproben entspricht) und jeweils 2 und 7 Tage nach Exposition analysiert. Die Majak-Arbeiter wurden in vier Strahlendosisgruppen (0 Gy, < 100 mGy, 100 – 500 mGy und > 500 mGy) eingeteilt und das Proteom der linken Herzkammer wurde mit markierungsfreier quantitativer Proteomik analysiert.

Die Proteomik-Profilierung der Kardiomyozyten und der menschlichen Herzproben zeigte Veränderungen im Spiegel der Proteine, die an kardialen Energiestoffwechselfunktionen beteiligt sind. In den menschlichen Proben wurden Veränderungen im mitochondrialen Stoffwechsel, in der Sirtuinsignalisierung und in der Reaktion auf oxidativen Stress beobachtet. Übereinstimmend mit den Ergebnissen unserer früheren Untersuchungen, zeigte die Analyse einen verringerten Spiegel im myokardialen Fettstoffwechsel, bei einer gleichzeitigen Reduktion des PPAR alpha, der eine Schlüsselrolle beim Herzmetabolismus spielt.

Diese Studie leistet einen wichtigen Beitrag zur Erforschung der Sirtuin / PGC1 / PPAR alpha-Signalwege bei strahlungsinduzierten Herzschäden.

Analysis of risks of cardiovascular diseases after radiation exposure at low doses in heart samples from Mayak nuclear workers (3617S32261)

ABSTRACT

Epidemiological studies show a significant increase in ischemic heart disease (IHD) incidence associated with total external gamma-ray dose among Mayak plutonium enrichment plant workers. Our previous studies using mouse and human heart samples suggest that persistent alteration of cardiac metabolism due to the inhibition of peroxisome proliferator-activated receptor (PPAR) alpha accompanies heart damage after high doses of ionising radiation. The aim of the present study was to further validate these findings using a cellular model (cardiomyocytes) and additional autopsy heart samples from a new set of Mayak workers.

Cardiomyocytes were cultured and irradiated with doses of 0 and 2 Gy approximately corresponding to the control and high-dose group in the human tissue samples and the analysis was performed 2 and 7 days after the radiation exposure. The Mayak workers were stratified into four radiation dose groups (0 Gy, <100 mGy, 100 - 500 mGy, and >500 mGy) and the proteome of the cardiac left ventricle was analysed using label-free quantitative proteomics.

Proteomics profiling of both cardiomyocytes and human heart samples revealed alterations in the level of proteins involved in the cardiac energy metabolism. In the human material, alterations in mitochondrial metabolism, sirtuin signalling and oxidative stress response were observed. In good agreement with our previous studies, the analysis showed decreased protein levels of myocardial lipid metabolism accompanied by a reduction in the level of active PPAR alpha, a key regulator of cardiac metabolism.

The study provides evidence for a marked contribution of the sirtuin/ PGC1/ PPAR alpha pathway to the radiation induced heart injury.

1 INTRODUCTION

Mayak Production Association (PA), located 150 km south-east of Ekaterinburg, is one of the biggest nuclear facilities in the Russian Federation. Individual dosimetric monitoring of external exposure performed at Mayak PA showed that the total external gamma-ray doses ranged widely from below 100 mGy to more than 5 Gy, with 32.6% of the workers having a total dose higher than 1 Gy. Epidemiological studies in this cohort showed a significant increase in ischemic heart disease (IHD) incidence associated with total external gamma-ray dose after correction for multiple competing factors such as smoking and alcohol consumption [1-3]. The risk estimates for IHD in relation to chronic external radiation dose are generally compatible with those reported in other large occupational studies and the Japanese A-bomb survivors [4].

Mitochondrial dysfunction plays a key role in the pathogenesis of IHD [5]. A high rate of mitochondrial catabolism of carbohydrates and fatty acids is crucial for furnishing the energy supply necessary for heart function. Under normal conditions the adult heart relies mostly on fatty acids for this energy production via the oxidative phosphorylation (OXPHOS) process, with only 10% to 30% of total ATP being derived from glucose. However, a normal heart can easily switch between fatty acids and glucose for ATP production, depending on energy demand and substrate availability [6]. In pathological conditions such as IHD this flexibility is lost and either superseded by a preference for glucose over fat [7] or an overall reduction of mitochondrial oxidative metabolism independent of the energy source [8]. Both scenarios are associated with the reduction in the level of active peroxisome proliferator-activated receptor (PPAR) alpha in cardiac ventricles [9]. PPAR alpha functions as a key regulator of cardiac metabolism and is essential for fatty acid oxidation [10]. We have previously shown that local heart irradiation in mice persistently decreases the respiratory capacity of cardiac mitochondria, reduces their number, and results in damage to the cristae structure [11]. Importantly, the activity of the transcription factor PPAR alpha is reduced by a dose-dependent increase in phosphorylation [11].

Although mouse models are widely used to study cardiac disease, there are functional differences between mouse and human hearts [12]. Infarction is virtually unknown in mice, probably due to their short life span, and differences in the heart physiology and diet. Even though mouse models have led to important observations on the causes of radiation-induced IHD, the question of their clinical relevance remains.

To address this issue, we have recently analysed the cardiac proteome response to irradiation in Mayak workers who were exposed only to external doses of gamma rays. Label-free quantitative proteomics analysis on tissue samples was performed from the cardiac left ventricles of Mayak workers stratified into four radiation dose groups (0 Gy, <100 mGy, 100 - 500 mGy, and >500 mGy) [13]. Our proteomic analysis revealed a dose-dependent series of alterations in the levels of proteins involved in the left ventricle function and structure. These included proteins critical for mitochondrial energy metabolism and cardiac cytoskeleton. A significant inactivation of PPAR alpha by phosphorylation was observed in the highest dose group (> 500 mGy) [13].

The objective of the present study was to further validate these findings by including an in vitro model using cardiomyocytes in cell culture, as well as inclusion of additional individuals in the study. The new cardiac samples originating from autopsies from both female and male individuals were analysed using proteomics, immunoblotting, and enzyme activity assays to verify the previous data.

The results presented here verified that alteration in the cardiac energy metabolism due to impaired PPAR alpha transcriptional activity contributes in radiation-induced cardiac damage. These data highlight the complexity of the PPAR alpha regulatory network and its cofactor PGC1.

2 SCIENTIFIC WORK PERFORMED AT SOUTHERN URAL BIOPHYSICS INSTITUTE (SUBI)

A new set of samples were provided as follows:

- Identification of the eligible persons for the study;
- Informed Consent signing;
- Collection of the epidemiological data for the study participants;
- *Post mortem* collection of the heart samples (fresh-frozen cuts and paraffin blocks of the left ventricle, and frozen cuts of the coronary artery) among the participants with known cumulative lifetime radiation dose and other clinical data (smoking, alcohol consumption, BMI);
- Shipment of the biological samples to Helmholtz Zentrum München (HMGU);
- Preparation of joint publications in peer-reviewed papers.

Identification of individuals for sampling was done using criteria of inclusion into and exclusion from the study agreed in 2011(FV 3611S30022), in particular, an individual was included into the study if:

- He/she was a Mayak worker predominantly exposed to external gamma-rays (worker) or was an Ozyorsk resident occupationally unexposed to radiation (control);
- He/she died from ischemic heart disease (IHD, ICD-9 codes 410–414) and/or was diagnosed with IHD more than once during lifetime;
- A measured plutonium body burden for him/her did not exceed 0.5 kBq (workers employed at the radiochemical or plutonium production plant).

An individual was excluded from the study if:

- He/she was exposed to internal alpha-radiation due to incorporated plutonium at high doses and no biophysical examination performed for those workers who could potentially be exposed to plutonium in the workplace (workers employed at the radiochemical and plutonium production plant) was carried out for him/her;
- He/she was diagnosed with cancer or other severe somatic disease.

Collection of fresh-frozen tissue samples from individuals meeting the requirements for inclusion in the study was done according to SOP agreed in 2011 before this study started (FV 3611S30022).

To achieve study objectives, individuals included in the study were divided into four groups by the total dose from external gamma-rays, i.e. controls (unexposed individuals), <100 mGy, 100–500 mGy and >500 mGy (Table1.2). For transfer of the samples to HMGU SUBI obtained a license for single transfer of biological samples. Fresh-frozen tissue samples and paraffin blocks were transferred to HMGU for the further molecular-genetic analysis in March 2018. Datasets for the epidemiological analyses were prepared.

Table 2-1 Number of individuals with available samples of fresh-frozen left ventricle tissue.

Controls (Ozyorsk residents)	Mayak workers				Total
	Controls (unexposed)	Total dose from external gamma-rays			
		<100 mGy	100-500 mGy	>500 mGy	
10	6	5	3	4	28

3 SCIENTIFIC STUDIES PERFORMED AT HELMHOLTZ ZENTRUM MÜNCHEN (HMGU)

3.1 MATERIALS AND METHODS

3.1.1 Cardiomyocytes

To better understand the signalling pathways altered by irradiation, a complementary cellular study was performed. Primary Human Cardiac Myocytes (HCM) (#12810; PromoCell) were purchased and cell culture conditions were established. The cardiomyocytes used in this study were originally isolated from the ventricles of the adult heart and are thus suitable for in vitro research on cardiac diseases and for pharmacological studies as well as long-term experiments.

The long-term effect of ionizing radiation on the viability of HCM was studied as follows: the cardiomyocytes were irradiated with doses of 0, 2, 4 and 8 Gy and the survival was analysed 7 days after exposure.

For the proteomics analysis, the cardiomyocytes were cultured and irradiated with doses of 0 and 2 Gy (approximately corresponding to the control and high-dose group in the human tissue samples) and the analysis was performed 2 and 7 days after radiation exposure.

3.1.2 Cardiac tissue

The individuals participating in this study were Mayak workers who were exposed occupationally to external gamma rays from 1949 onward at the Mayak Production Association [2, 14]. The controls were either non-Mayak workers living in the same area (Ozyorsk residents) or non-exposed Mayak workers. The workers and the controls were all diagnosed with multiple IHDs during lifetime and also died due to IHD. The heart tissues were collected by autopsy. Detailed information on the sample donors is presented in 1.1 and 2.1.

The heart tissues were collected from 28 individuals representing four dose groups as follows: 16 individuals (10 females and 6 males) as controls, 7 individuals (4 females and 3 males) from the dose group <100 mGy, 3 individuals (males) representing doses between 100 - 500 mGy, and 4 individuals (3 males and 1 female) from the dose group >500 mGy.

Table 3-1 Detailed information on the sample donors. The samples in italics represent cardiac autopsies from females collected in the previous project (FV 3611S30022) and included in the new analysis in order to generate stronger statistics.

№	Sample ID	"Clinic" database ID	worker or control	Gender	Date of birth	Date of death	Total body dose, mGy
1	52	88546	control	female	25/03/1929	28/09/2014	0
2	54	14011	worker	male	10/04/1935	15/04/2015	1226.5
3	55	89110	worker	male	01/08/1950	17/04/2015	0
4	56	36995	worker	male	07/11/1958	19/04/2015	0
5	57	78590	control	female	16/12/1945	19/05/2015	0
6	58	61028	control	female	20/10/1936	21/05/2015	0
7	59	3390	worker	male	20/09/1935	31/05/2015	1154.3
8	61	15213	worker	male	15/07/1929	03/06/2015	1426.0
9	63	37671	worker	male	16/12/1942	23/10/2015	103.4
10	65	35491	worker	male	10/07/1938	22/11/2015	9.8
11	66	27766	worker	male	17/05/1957	23/11/2015	0.3
12	67	4660	worker	male	26/05/1968	23/01/2016	0
13	68	63173	control	male	31/03/1960	26/03/2016	0
14	69	34521	worker	female	16/12/1948	28/03/2016	0.5
15	70	38551	worker	male	05/05/1966	10/05/2016	0
16	71	22206	worker	male	04/02/1938	13/05/2016	21.6
17	73	38591	worker	female	29/05/1955	15/05/2016	0
18	74	90293	control	female	25/09/1928	04/06/2016	0
19	76	90413	control	female	07/12/1948	03/08/2016	0
20	78	90669	control	female	06/12/1948	15/11/2016	0
21	79	37325	worker	male	19/06/1935	10/04/2017	92.8

№	Sample ID	"Clinic" database ID	worker or control	Gender	Date of birth	Date of death	Total body dose, mGy
22	80	49574	control	female	30/01/1930	10/04/2017	0
23	81	26731	worker	male	09/05/1945	14/04/2017	196.7
24	82	91398	control	female	23/07/1934	05/06/2017	0
25	84	61295	control	female	24/07/1947	16/06/2017	0
26	85	19606	worker	male	15/10/1941	20/06/2017	409.9
27	86	81113	worker	male	25/09/1954	12/08/2017	0
28	87	16366	worker	female	30/11/1929	25/09/2017	1304.8
29	*49*	*53136*	*control*	*female*	*1.7.1938*	*30.3.2014*	*0*
30	*32*	*59222*	*control*	*female*	*26.10.1937*	*24.6.2013*	*0*
31	*30*	*62286*	*control*	*female*	*22.2.1931*	*14.4.2013*	*0*
32	*9*	*89*	*control*	*female*	*18.10.1931*	*18.4.2012*	*0*
33	*51*	*27686*	*worker*	*female*	*27.1.1945*	*30.8.2014*	*71.0*
34	*6*	*36267*	*worker*	*female*	*21.11.1931*	*11.4.2012*	*54.0*

3.1.3 Cell viability and proliferation assays

The cell proliferation was monitored by the WST-1 assay with a microplate reader (BioTek, µQuant Microplate Spectrophotometer) according to the manufacturer's protocol. The WST-1 assay works based on the cleavage of the stable tetrazolium salt (WST-1) to a soluble formazan by a complex cellular mechanism largely dependent on the glycolytic production of NAD(P)H in viable cells. Therefore, the amount of formazan dye formed directly correlates to the number of metabolically active cells in the culture.

The cells grown in a 96-well tissue culture plate are incubated with the WST-1 reagent for 0.5 - 4 hours. After this incubation period, the formazan dye formed is quantitated with a scanning multi-well spectrophotometer (ELISA reader). The measured absorbance directly correlates to the number of viable cells.

3.1.4 Proteomics analysis

Considerable heterogeneity of the heart samples made classical proteomics profiling of pool or paired samples problematic. To address this problem, all the samples were analysed by label free quantification. The platform enabled us to analyse the individual and independent proteome profile of each sample. The samples were lysed as described before [13, 15].

To lyse the tissue, frozen heart was ground to a fine powder with a cold (-20°C) mortar and pestle before suspending in lysis buffer (SERVA). Protein concentration was determined by Bradford assay following the manufacturer's instructions (Thermo Fisher).

The protein lysates were digested to the peptides using trypsin and impurities were removed [16] as follows: an aliquot containing 10 µg of protein was digested using a modified FASP procedure. In brief, the proteins were reduced and alkylated using DTT and IAA and then centrifuged through a 30 kDa cut-off filter device (PALL, Port Washington, USA), washed three times with UA buffer (8 M urea in 0.1 M Tris/HCl pH 8.5) and

twice with 50 mM AmBic. The proteins were digested for 2 hours at room temperature using 1 µg Lys-C (Wako Chemicals, Neuss, Germany) and for 16 hours at 37°C using 2 µg trypsin (Promega, Mannheim, Germany). The peptides were collected by centrifugation (10 min at 14 000 g), and the samples were acidified with 0.5% TFA and stored at -20°C.

The generated peptides were solved directly before LC-MS/MS analyses in 2 % ACN / 0.5 % TFA and separated by reversed phase chromatography (PepMap, 15 cm x 75 µm ID, 3 µm/100Å pore size, LC Packings) operated on a nano-HPLC (Ultimate 3000, Dionex) with a nonlinear 170 min gradient using 2% acetonitrile in 0.1% formic acid in water (A) and 0.1% formic acid in 98% acetonitrile (B) as eluents with a flow rate of 250 nl/min. The gradient settings were as follows: 0 to 140 min: between 2% and 5% to 31% B; 140 to154 min: 31% to 95% B; 145 to150 min: constant at 95% B; 150-155 min 95% to 5% B.

The nano-LC was connected to a linear quadrupole ion trap mass spectrometer (LTQ Orbitrap XL, ThermoFisher, Bremen, Germany) equipped with a nano-ESI source. The mass spectrometer was operated in the data-dependent mode to automatically switch between Orbitrap-MS and LTQ-MS/MS acquisition. Survey full scan mass spectra (from m/z 300 to 1500) were acquired in the Orbitrap with a resolution of R = 60,000 at m/z 400 (after accumulation to a target of 1,000,000 charges in the LTQ-MS/MS). This method allowed up to 10 of the most intense ions to be isolated sequentially, depending on signal intensity, for fragmentation on the linear ion trap using collision-induced dissociation at a target value of 100,000 ions. High resolution MS scans in the Orbitrap and MS/MS scans in the linear ion trap were performed in parallel. Target peptides already selected for MS/MS were dynamically excluded for 30 seconds. General mass spectrometry conditions were: electrospray voltage from 1.25 kV to 1.4 kV; no sheath and auxiliary gas flow. Ion selection threshold was 500 counts for MS/MS, and an activation Q-value of 0.25 and activation time of 30 ms were applied for MS/MS.

The acquired spectra (Thermo raw files) were loaded into the Progenesis software (version 3.0, Nonlinear) and label-free quantification was performed as described before [13, 17]. Features with only one charge or more than X charges were masked and excluded from further analyses and all remaining features were used to calculate a normalization factor for each sample that corrects for experimental variation. Samples were then allocated to their experimental group (control or irradiated). For quantification, all unique peptides (with Mascot score ≥ 30 and $p < 0.01$, see below) of an identified protein were included and the total cumulative abundance was calculated by summing the abundances of all peptides allocated to the respective protein. No minimal thresholds were set for the method of peak picking or selection of data to use for quantification. Statistical analysis was performed using the "between subject design" and p-values were calculated by a repeated measures analysis of variance (ANOVA) using the sum of the normalized abundances across all runs.

MS/MS spectra were exported from the Progenesis software as Mascot Generic file (mgf) and used for peptide identification with Mascot (version 2.2) in the Ensembl database for human containing a total of 54,576 sequences. The following search parameters were used: 10 ppm peptide mass tolerance and 0.6 Da fragment mass tolerance, one missed cleavage was allowed, carbamidomethylation (C) was set as fixed modification and oxidation (M), deamidation (N, Q) were allowed as variable modifications. Mascot integrated decoy database search calculated a false discovery of ≤ X% when searching was performed on the concatenated mgf files with an ion score cut-off of 30 and a significance threshold of $p \leq 0.01$. Only peptides with ion scores of 30 and above as well as proteins with at least one unique peptide ranked as top candidate (bold red in Mascot) were considered and re-imported into Progenesis software. For each dataset, the peptide assignments were re-imported into the Progenesis LC MS software. After summing up the abundances of all of the peptides, they were allocated to each protein.

3.1.5 Protein-protein interaction and signalling network

The analyses of protein-protein interaction and signalling networks were performed by the software tools STRING 10.5 (http://string-db.org) and INGENUITY Pathway Analysis (IPA) (INGENUITY System, http://www.INGENUITY.com). IPA is a knowledge database generated from peer-reviewed scientific publications that enables discovery of highly represented functions and pathways ($p < 0.001$) from large quantitative data sets [18].

3.1.6 Immunoblot analysis

Protein lysates from pooled samples were analysed by immunoblotting. For pooled samples, similar amounts of protein from each individual belonging to the same radiation dose group (control, <100 mGy, 100 - 500 mGy and >500mGy) were combined into a batch representing that group. Proteins separated by 4-12% SDS-PAGE were transferred to nitrocellulose membranes (GE Healthcare) using a TE 77 semidry blotting system (GE

Healthcare) at 1 mA/cm for 1h. The membranes were blocked using 3 % BSA in TBS, pH 7.4, for 1 h at room temperature, washed three times in 10 mM Tris-HCl, pH 7.4, 150 mM NaCl for 5 min and incubated overnight at 4 °C with primary antibodies using dilutions recommended by the manufacturer. Immunoblot analysis of heart protein lysate was performed using anti-SIRT1 (#9475S; cell signalling), anti-SIRT2 (#12650; cell signalling), anti-SIRT3 (#5490; cell signalling), anti-SIRT4 (Santa Cruz Biotechnology), anti-SIRT5 (sc-271635; Santa Cruz Biotechnology), anti-SIRT6 (Santa Cruz Biotechnology), anti-SIRT7 (sc-365344; Santa Cruz Biotechnology), anti-PGC1 (E-AB-13508; Biomol), anti-PPAR alpha (sc-9000; Santa Cruz Biotechnology), anti-phospho-PPAR alpha, S-12 (ab3484; abcam), anti-acetylated lysine (#9441; cell signalling), anti-NRF2 (sc-365949; Santa Cruz Biotechnology), anti-GSTK1 (sc-515580; Santa Cruz Biotechnology), anti-CAT (ab52477; abcam). After washing three times, the blots were incubated with the appropriate horseradish peroxidase-conjugated or alkaline phosphatase-conjugated anti-mouse, anti-rabbit or anti-goat secondary antibody (Santa Cruz Biotechnology) for 2 h at room temperature and developed using the ECL system (GE Healthcare) or 1-stepTM NBT/BCIP method (ThermoFisher) following standard procedures. Reversible Ponceau staining was used as the loading control. For immunoprecipitation, 100 µg of extract from pooled samples was incubated overnight with control IgG or PGC1 antibody; the mixed reaction were precipitated with Protein A /G Agarose beads (Santa Cruz Biotechnology) according to the manufacturer's instructions and immunoprecipitates were analysed by Western blot.

Quantification of digitised images of immunoblot bands was done using ImageJ (http://rsbweb.nih.gov/ij/). Three replicates of control and irradiated samples for each treatment were used for quantification.

3.1.7 NAD/ NADH assay

Nicotinamide adenine dinucleotide (NAD) in an oxidized form, NAD+, or a reduced form, NADH functions in modulating cellular redox status and by controlling signalling in physiological and pathological events. Cardiac NAD/NADH levels were quantified with a commercially available kit (MAK037, Sigma Chemical, St. Louis, MO, United States) according to the manufacturer's instructions.

3.1.8 Statistical analysis

The student´s t-test (unpaired) was used as statistical tests. Group difference was considered as statistically significant with values of $p^* < 0.05$, $p^{**} < 0.01$. The error bars were calculated as standard error of the mean (SEM).

4 RESULTS

4.1 RADIATION EFFECT ON CELL PROLIFERATION AND VIABILITY

We performed a WST-1 cellular proliferation assay on cardiomyocytes after radiation exposure. The irradiated groups demonstrated a significant decrease in mitochondrial NADH dehydrogenase activity as compared to the controls (0 Gy), confirming that the cellular metabolism is affected by irradiation. The effect seems to be level of at 2 Gy and does not show a dose-dependent decline.

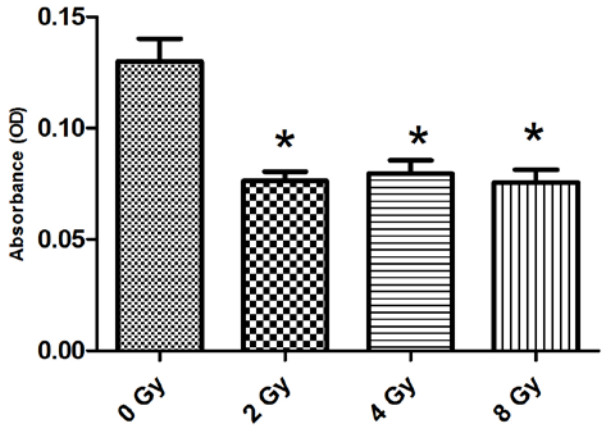

Figure 4-1 Cell viability of cardiomyocytes after irradiation. WST-1 cellular proliferation assay was performed on the cardiomyocytes after radiation exposure. The cell viability is presented as absorbance (mean ± SD) compared to the non-exposed control.

4.2 RADIATION RESPONSE IN THE CARDIOMYOCYTE PROTEOME

To study the proteome response of cardiomyocytes to radiation exposure, five biological replicates of cardiomyocytes irradiated using the doses of 0 and 2 Gy were harvested 2 and 7 days after exposure, lysed and subjected to quantitative proteomics analysis as described before. The label-free quantification proteomics data were further combined in a bioinformatics analysis using software tools INGENUITY and STRING.

Proteomics analysis of cardiomyocytes identified 3286 proteins in total. More than 67% of these proteins were quantified by at least 2 unique peptides. Proteins identified by a minimum of 2 unique peptides and having fold changes greater than 1.30-fold or less than 0.77-fold (p-values <0.05) were considered as significantly differentially expressed. The analysis showed that 19 proteins were significantly changed in the irradiated cells (2 Gy) after 2 days. The number of changed proteins increased after 7 days to 225. This suggests a time-dependent increase in the number of altered proteins. Eight deregulated proteins were shared between the two time point groups (Figure 4-2). These 8 proteins could not be categorised under any common molecular function.

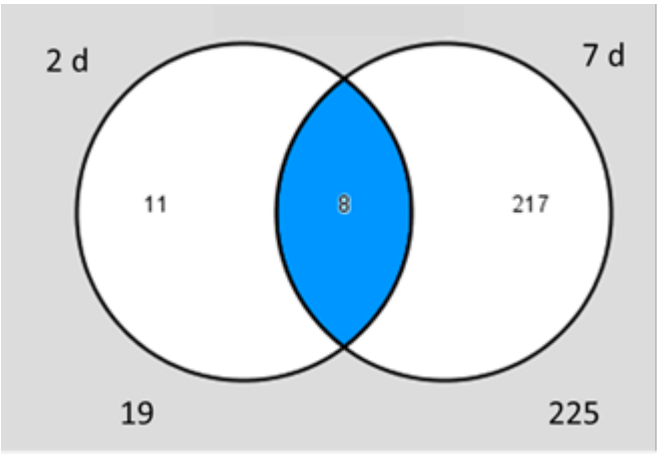

Figure 4-2 Radiation-induced alteration in the cardiomyocyte proteome. (A) The Venn diagram shows the number of total and shared deregulated proteins 2 and 7 days (d) after exposure to 2 Gy compared to control (0 Gy).

A detailed analysis of the functional interactions and biological pathways was performed using IPA software (http://www.INGENUITY.com). Mitochondrial dysfunction, sirtuin signalling, and PPAR/ RXR signalling were the mostly affected pathways in irradiated cells compared to the control group at both time points (Figure 4-3).

Figure 4-3 Pathway analysis of significantly differentially expressed proteins in irradiated cardiomyocytes. A dose-dependent alteration is observed in the pathways involved in energy production. The pathway scores are displayed using a purple colour gradient, where darker purple corresponds to higher scores (increased statistical significance). By default, the rows (pathways) with the highest total score across the set of observations are sorted to the top (http://www.INGENUITY.com).

Furthermore, the analysis predicted inhibition of transcription factors such as PPAR alpha, in irradiated cells (7 days after exposure) suggesting an alteration in metabolism after irradiation. The predicted inactivation of PPAR alpha after 7 days was confirmed by immunoblotting showing that the ratio of phosphorylated (inactive) PPAR alpha to total protein was slightly but not significantly increased in irradiated cells after 7 days (Figure 4-4A). The ratio of phosphorylated PPAR alpha to total protein remained unchanged in all irradiated samples after 2 days (Figure 4-4B and C).

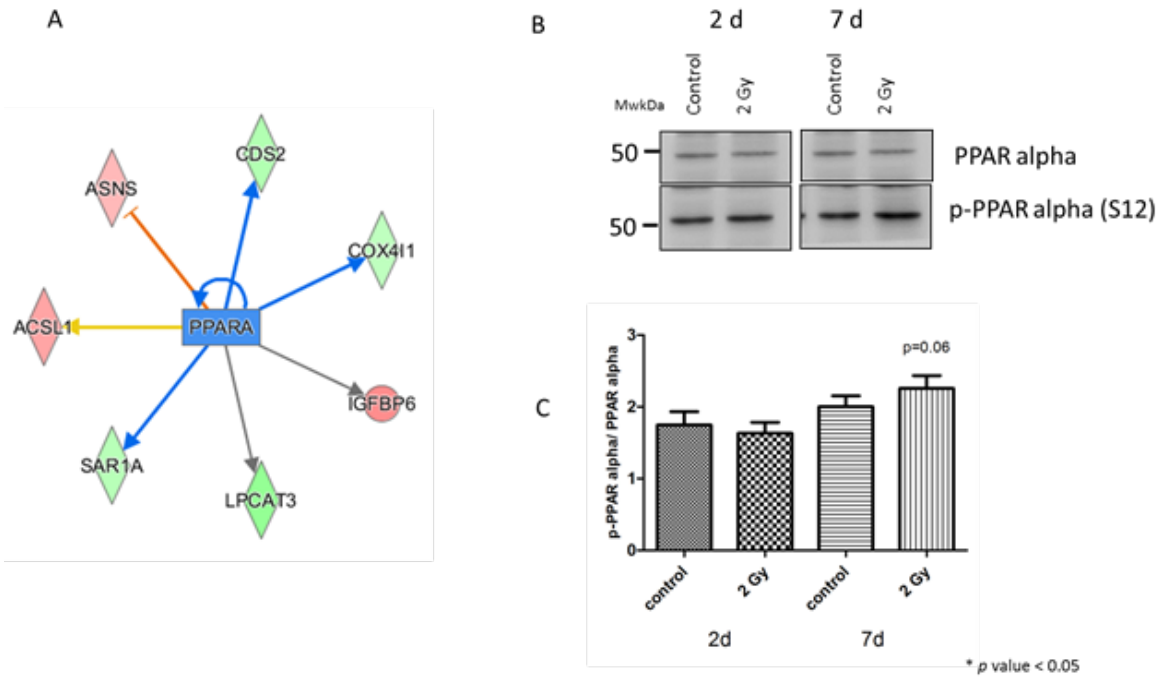

Figure 4-4 Analysis of the activation status of PPAR alpha. IPA prediction of inactivation of PPAR alpha based on the deregulated proteins from proteomics analysis in the cardiomyocytes 7d after exposure to 2 Gy (A) (http://www.INGENUITY.com). Immunoblotting analysis of PPAR alpha total and phosphorylated proteins is shown (B). The columns represent the average ratios of relative protein expression in control and irradiated samples after background correction (C). The amount of the total protein was measured by Ponceau S staining for accurate comparison between the groups. The error bars represent standard error of the mean (+ SEM) (t-test; *p< 0.05; n=3).

4.3 RADIATION RESPONSE IN THE HEART PROTEOME

4.3.1 Male hearts

The proteomics analysis of male hearts identified 1912 proteins in all four groups, of which 924 proteins were identified by at least 2 unique peptides. Among the quantified proteins, 75, 102 and 127 proteins were significantly changed (+1.3-fold; p<0.05) after <100 mGy, 100-500 mGy and >500 mGy exposure, respectively, suggesting a dose-dependent increase in the number of altered proteins; only 4 deregulated proteins were shared between the three exposed groups (Figure 4-5).

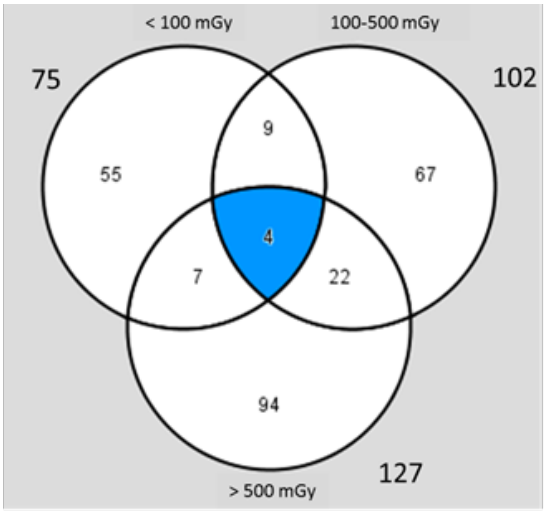

Figure 4-5 Radiation-induced alteration in the cardiac proteome. The Venn diagram shows the number of total and shared deregulated proteins in the dose groups <100 mGy, 100-500 mGy and >500 mGy compared to control (0 Gy) (http://www.INGENUITY.com).

A detailed analysis of the functional interactions and biological pathways was performed using IPA software (http://www.INGENUITY.com). Mitochondrial function and metabolic pathways such as sirtuin signalling, and Krebs cycle (TCA cycle) were the most affected pathways in all irradiated groups compared to the controls (Figure 4-6).

Figure 4-6 Pathway analysis of significantly differentially expressed proteins in irradiated cardiomyocytes. A dose-dependent alteration is observed in the pathways involved in energy production. The pathway scores are displayed using a purple colour gradient, where darker purple corresponds to higher scores (increased statistical significance). By default, the rows (pathways) with the highest total score across the set of observations are sorted to the top (http://www.INGENUITY.com).

A dose-dependent reduction in expression of proteins of the respiratory complexes was found. The number of deregulated mitochondrial proteins increased with radiation dose (Figure 4-7).

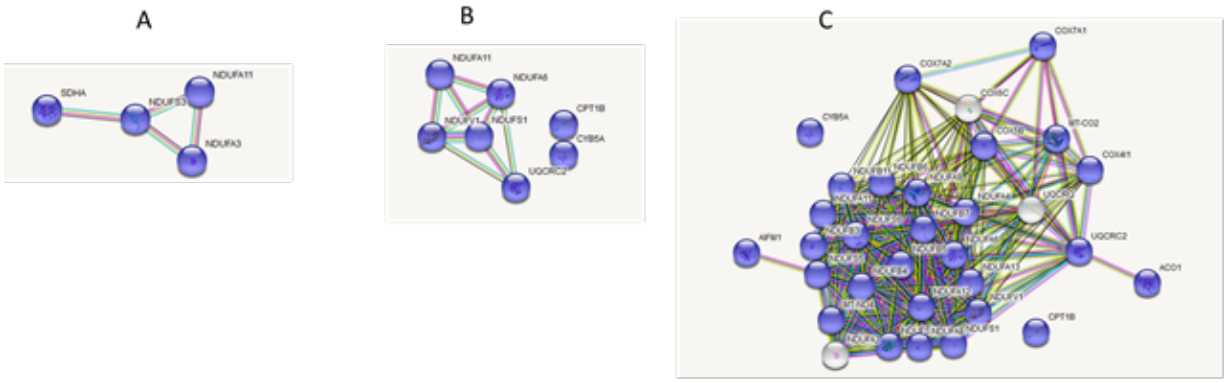

Figure 4-7 Protein network analysis of significantly differentially expressed mitochondrial proteins. Protein-protein interaction analysis of the significantly differentially expressed proteins showing the networks of deregulated mitochondrial proteins in the dose groups <100 mGy (A), 100-500 mGy (B) and >500 mGy (C) (http://string-db.org).

Downregulation of several proteins of the mitochondrial complex I may result in reduced NAD production and subsequently alter the sirtuin signalling. The NAD/NADH assay showed significantly increased levels of NADH resulting in decreased NAD/NADH ratios in the dose group > 500 mGy (Figure 4-8).

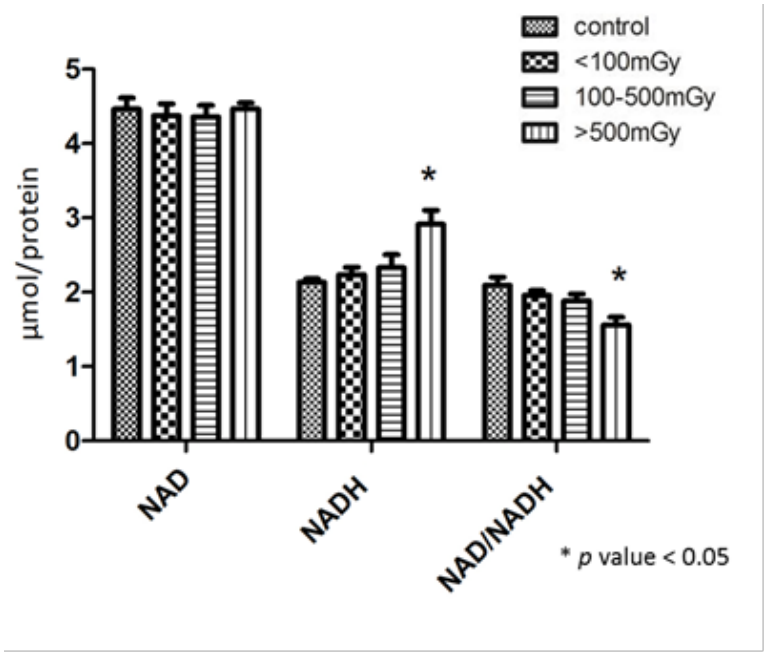

Figure 4-8 Analysis of the NAD, NADH and NAD/NADH in different dose groups. The concentration of NAD, NADH and NAD/NADH were compared in pooled samples from irradiated and control groups. The error bars represent standard error of the mean (+ SEM) (t-test; *p< 0.05; n=3).

According to the Ingenuity Pathway Analysis (IPA), the majority of deregulated proteins were participating in sirtuin signalling pathway. To investigate which sirtuin isoform was affected in irradiated hearts, we analysed the protein expression of sirtuins by immunoblotting (Figure 4-9A and B). The analysis indicated a significant downregulation of sirtuins located in the mitochondria (SIRT3, SIRT4 and SIRT5) in the dose group > 500 mGy (Figure 4-9B).

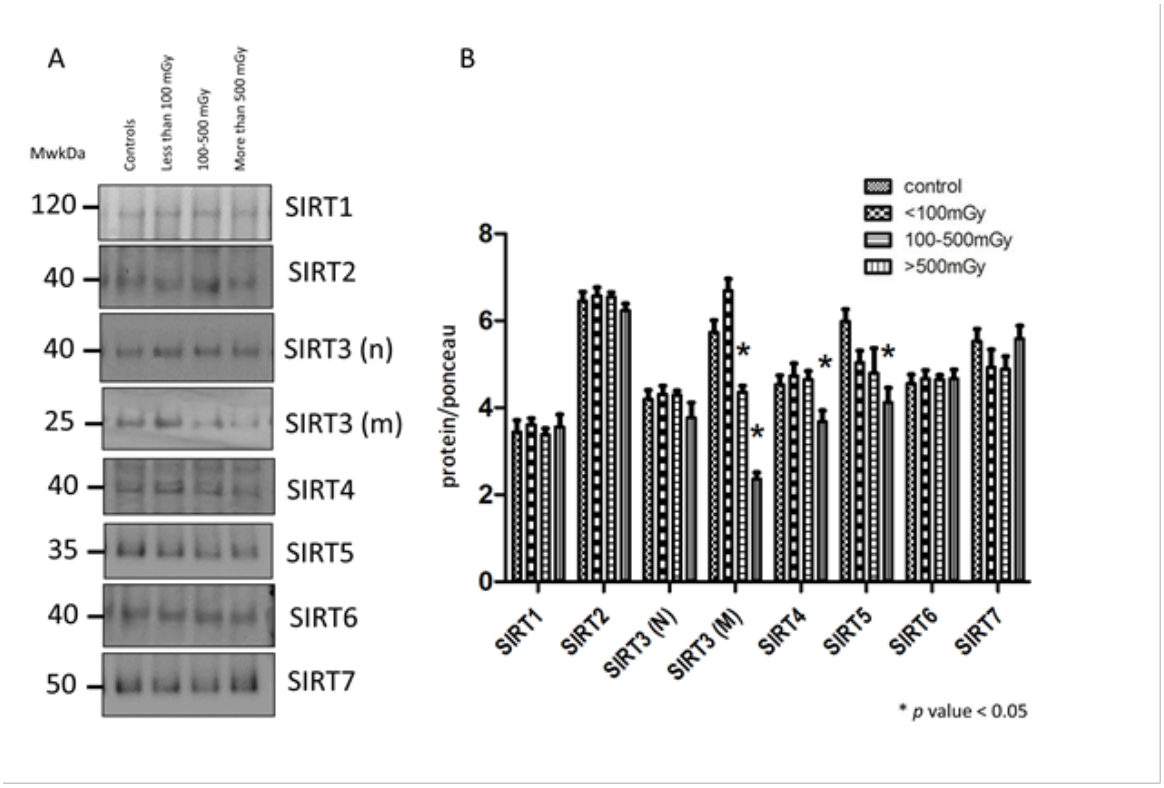

Figure 4-9 Analysis of the sirtuin expression. Immunoblotting analysis of SIRT1, SIRT2, SIRT3 (nuclear = n), SIRT3 (mitochondrial = m), SIRT4, SIRT5, SIRT6, and SIRT7 was performed (A). The columns represent the average ratios of relative protein expression in control and irradiated samples after background correction (B). The amount of the total protein was measured by Ponceau S staining for accurate comparison between the groups. The error bars represent standard error of the mean (+ SEM) (t-test; *p< 0.05; n=3).

Based on the IPA upstream regulator analysis, PPAR alpha was predicted to be inhibited in irradiated groups (100 - 500 mGy and > 500 mGy) (Figure 4-10A and B). The activity of PPAR alpha in the cardiac tissue depends on the phosphorylation of Ser12, increased phosphorylation meaning deactivation of this transcription factor [19]. The ratio of phosphorylated (inactive) to total protein was significantly increased in irradiated samples compared to the control group (Figure 4-10C and D) suggesting radiation-related reduction of PPAR alpha transcriptional activity in irradiated groups. As PPAR alpha is the transcription factor for many enzymes essential in fatty acid metabolism, this is in good agreement with the observed downregulation of these PPAR alpha target proteins such as carnitine O-palmitoyltransferase (CPT), acetyl-CoA acetyltransferase (ACAT1), and long-chain (S)-3-hydroxyacyl-CoA (HADHA) (Figure 4-10A and B).

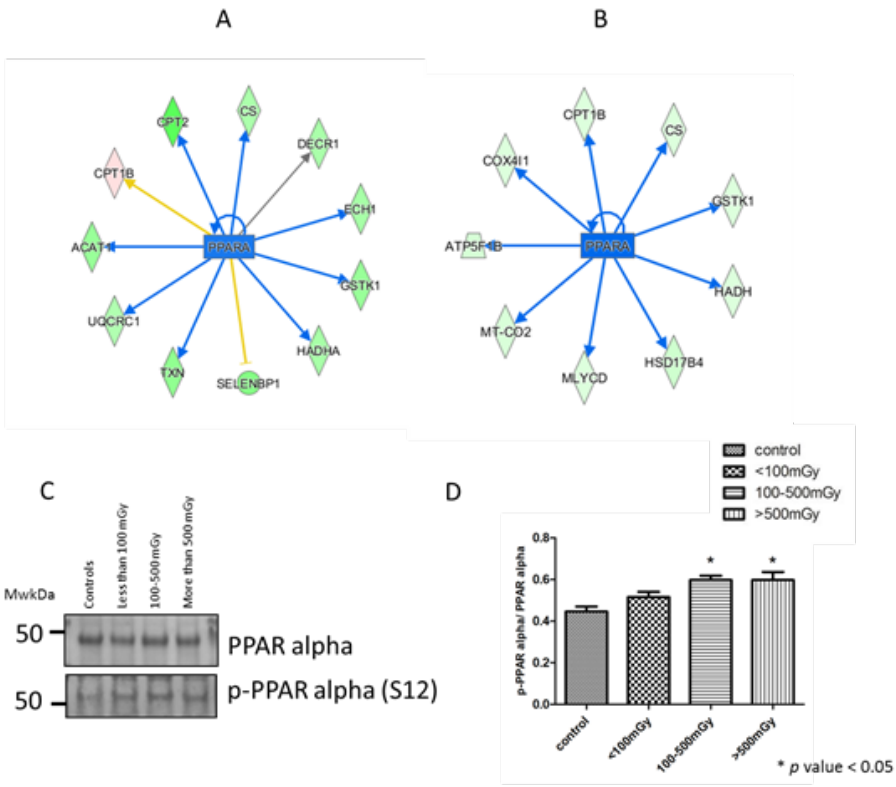

Figure 4-10 Analysis of the activation status of PPAR alpha. Predicted inactivation of PPAR alpha based on the deregulated proteins in the dose groups 100 - 500 mGy (A) and > 500mGy (B) (http://www.INGENUITY.com) is shown. The upregulated proteins are marked in red and the downregulated in green. The blue colour of the node (PPAR alpha) indicates inactivation. Immunoblot analysis of total and phospho-PPAR alpha (Ser12) in pooled samples is shown (C). The columns represent the average ratios of relative protein expression in control and irradiated samples (D). The amount of the total protein was measured by Ponceau S staining for accurate comparison between the groups. The error bars represent standard error of the mean (+ SEM) (t-test; *p< 0.05; n=3).

In addition, PGC1, a central regulator of the mitochondrial biogenesis [20] and a cofactor needed for the activation of PPAR alpha [21] was predicted to be inactive (figure 4-11A and B). As PGC1 is regulated by SIRT1 via acetylation/deacetylation, the expression level of PGC1 and its acetylated (inactive) form was examined in irradiated and control samples. The results confirmed the significantly enhanced level of acetylated PGC1 in irradiated groups (Figure 4-11C and D). Although there was no prediction of PGC1 activity for group < 100 mGy, we still found the increased level of PGC1 acetylation (Figure 4-11C and D).

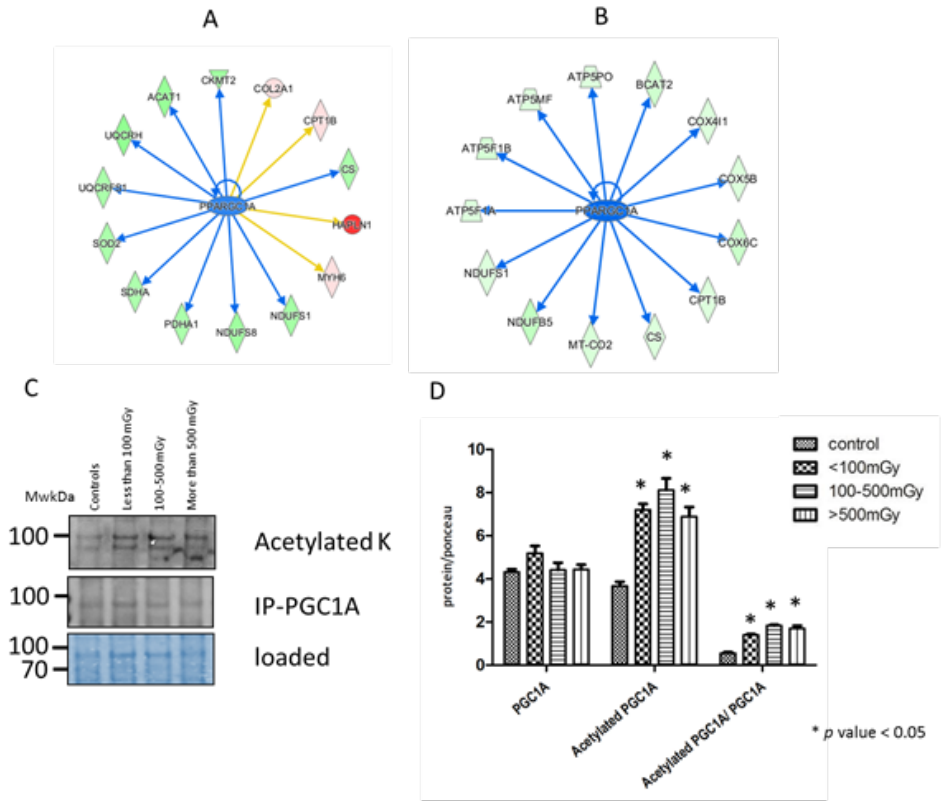

Figure 4-11 Analysis of the activation status of PGC1. Predicted inactivation of PGC1 based on the deregulated proteins in the dose groups 100 - 500 mGy (A) and > 500mGy (B) (http://www.INGENUITY.com) is shown. There was no prediction for group < 100 mGy. The upregulated proteins are marked in red and the down-regulated in green. The blue colour of the node (PGC1) indicates inactivation. Immunoblot analysis of total PGC1, and acetylated form (inactive) in pooled samples is shown (C). The columns represent the average ratios of relative protein expression in control and irradiated samples (D). The amount of the total protein was measured by Ponceau S staining for accurate comparison between the groups. The error bars represent standard error of the mean (+ SEM) (t-test; *p< 0.05; n=3).

The analysis also showed the downregulation of proteins involved in the oxidative stress response such as catalase (CAT), glutathione s-transferase (GSTK1) and thioredoxin in irradiated samples. Consistent with the proteomics data, immunoblotting showed markedly decreased levels of proteins CAT, and GSTK1 after irradiation (Figure 4-12). However, the expression of transcription factor NRF2, the central regulator of the anti-oxidative response, remained unchanged in irradiated samples (Figure 4-12).

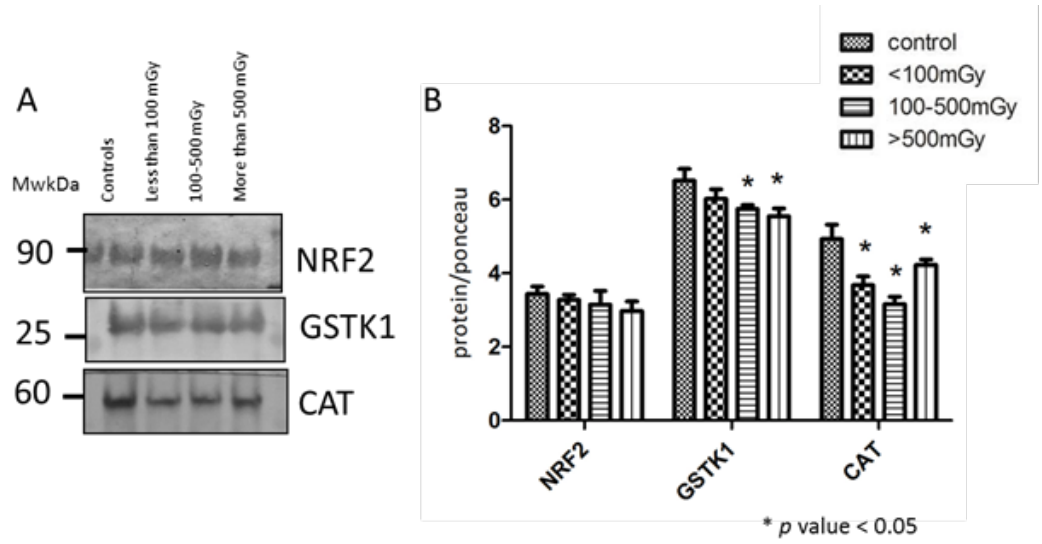

Figure 4-12 Analysis of the oxidative stress response proteins. Immunoblot analysis of NRF2, GSTK1 and CAT in pooled samples is shown (A). The columns represent the average ratios of relative protein expression in control

and irradiated samples (B). The amount of the total protein was measured by Ponceau S staining for accurate comparison between the groups. The error bars represent standard error of the mean (+ SEM) (t-test; *p< 0.05; n=3).

4.3.2 Female hearts

The proteomics analysis of female hearts identified 1941 proteins in all four groups, of which 1135 proteins were identified by at least 2 unique peptides. Among the quantified proteins, 49 proteins were significantly changed (+1.3-fold; p<0.05) after < 100 mGy exposure. A detailed analysis of the functional interactions and biological pathways was performed using the IPA software (http://www.INGENUITY.com). Mitochondrial dysfunction, sirtuin signalling, and EIF2 signalling were the most affected pathways in the irradiated group compared to the controls (Figure 4-13).

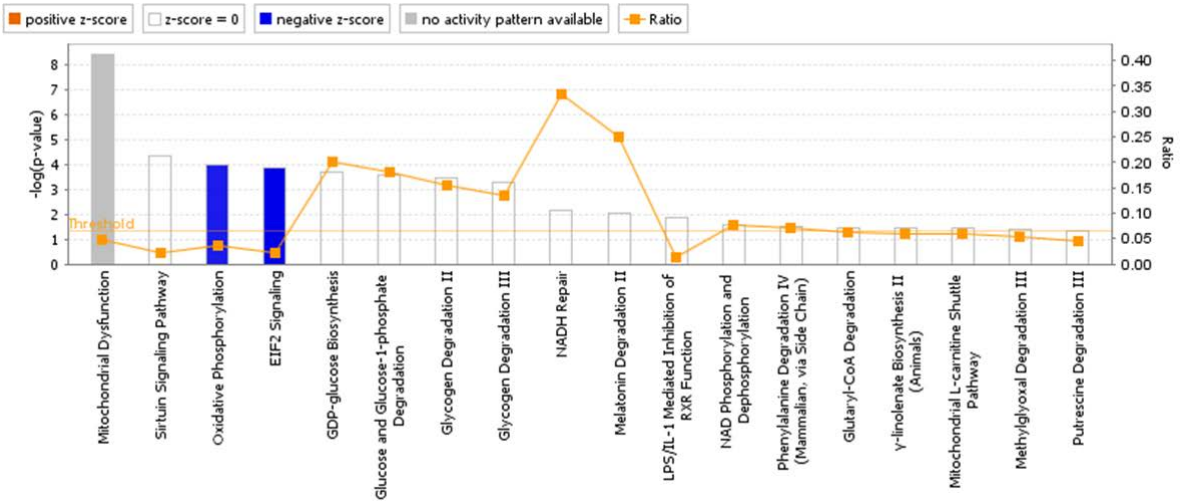

Figure4-13 Pathway analysis of the significantly differentially expressed proteins in irradiated female samples. Bars indicate canonical pathways and y-axis displays the – (log) significance. Taller bars are more significant than shorter bars. The blue colour (a negative z-score) indicates potential inhibition of the pathway (http://www.INGENUITY.com).

As we had only one heart sample from a female individual exposed to dose > 500 mGy, no statics could be provided for this analysis. To make a profile for this individual, the heart proteome was only filtered for fold changes among proteins identified by at least 2 unique peptides. The comparison analysis showed dose-dependent effect of irradiation on cardiac metabolic pathways (Figure 4-14).

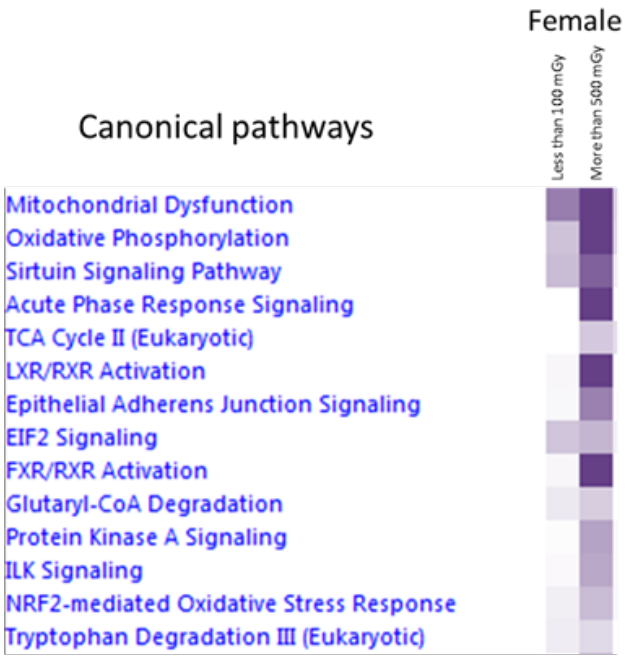

Figure 4-14 Pathway analysis of significantly differentially expressed proteins in irradiated female samples. A dose-dependent alteration is observed in the pathways involved in the cardiac metabolism. The pathway scores are displayed using a purple colour gradient, where darker purple corresponds to higher scores (increased statistical significance). By default, the rows (pathways) with the highest total score across the set of observations are sorted to the top (http://www.INGENUITY.com).

5 DISCUSSION

5.1 COMPARISON OF CARDIOMYOCYTE AND HEART TISSUE PROTEOME CHANGES AFTER IRRADIATION

In the present study, we investigated, in addition to the human heart samples from Mayak workers exposed to a range of external radiation doses, the proteome response of cardiomyocytes to irradiation as a cellular model for irradiated heart. Although the comparison between proteome response of the chronically irradiated cardiac tissue and the acutely irradiated cardiac cells is not directly possible, both in vivo and in vitro scenarios showed similar response to irradiation (Figure 15). Mitochondrial proteins represented the most sensitive protein group in both cases. The most affected biological pathways were mitochondrial dysfunction, oxidative phosphorylation, and sirtuin signalling. Furthermore, bioinformatics analysis predicted reduced activity of PPAR alpha in both cardiomyocytes and cardiac tissue suggesting that the cardiac cells analysed in the present study can be used as a suitable cellular model for further investigations.

Figure 5-1 Comparison of affected pathways in irradiated cardiomyocytes and male cardiac samples. The cellular and tissue proteome profiles show similar patterns of biological pathways involved. The pathway scores are displayed using a purple colour gradient, where darker purple corresponds to higher scores (increased statistical significance). By default, the rows (pathways) with the highest total score across the set of observations are sorted to the top (http://www.INGENUITY.com).

5.2 COMPARISON OF MALE AND FEMALE CARDIAC PROTEOME CHANGES AFTER IRRADIATION

The comparison analysis between female and male cardiac proteome responses to irradiation showed strong similarity between different gender profiles (Figure 5-2). The mitochondrial dysfunction, oxidative phosphorylation, and sirtuin signalling were affected in a dose-dependent manner in both male and female samples.

Figure 5-2 Comparison of affected pathways in irradiated female and male cardiac tissues. The female and male proteome profiles show similar patterns of biological pathways involved. The pathway scores are displayed using a purple colour gradient, where darker purple corresponds to higher scores (increased statistical significance). By default, the rows (pathways) with the highest total score across the set of observations are sorted to the top (http://www.INGENUITY.com).

The proteomics data showed a significant radiation-induced dose-dependent alteration of the proteins involved in the cardiac mitochondrial energy metabolism. In agreement with our previous data obtained in mouse models [11, 15, 22-24] and human [13], the proteomics analysis showed downregulation of several mitochondrial proteins. In particular, the expression of proteins belonging to mitochondrial complexes I and III were significantly downregulated. We have previously reported that local heart irradiation in mice induces persistent functional and proteome alterations in cardiac mitochondria that are associated with reduced activity of complexes I and III [24]. Ischemic damage to the heart is also associated with defaults in the activity of complexes I and III [25, 26]. Cardiac mitochondria are key players in the physiology and pathology of the heart. The role of mitochondrial dysfunction in cardiovascular disease has been well described [8, 27, 28]. The downregulation of mitochondrial complex I results in reduced activity of this complex, increased reactive oxygen species production and changes in the NAD+/NADH balance [29]. In good agreement with this, we found significant accumulation of NADH and reduction in the NAD+/NADH ratio in male hearts in the high-dose male group (> 500 mGy).

The NAD+/NADH ratio regulates various metabolic pathways including fatty acid oxidation, Krebs cycle, and glycolysis [30]. The bioinformatics analysis of proteomics profiles predicted that radiation-induced metabolic alteration may result from the deactivation of PPAR alpha. PPAR alpha that is highly expressed in tissues with

elevated metabolic turnover is the main transcriptional regulator of cardiac fatty acid oxidation genes, lipoprotein assembly and lipid transport [10, 31, 32]. We have previously shown that high-dose radiation is able to alter cardiac fatty acid oxidation and results in increased systemic inflammation in mice that were exposed locally at the heart with X-ray doses of 8 and 16 Gy (16 weeks post-exposure) [11]. Similar findings were observed in humans. In our previous study on the male Mayak workers (project FV 3611S30022), we showed an inactivation of PPAR alpha in cardiac left ventricle investigated post mortem [13]. Our data suggested that the persistent alteration of cardiac metabolism is accompanied with and probably a result of impaired PPAR alpha activity [11].

Proteomics profiling of male hearts showed deregulation of a cluster of proteins involved in sirtuin signalling. Sirtuins are a family of NAD+-dependent deacetylases and ADP-ribosyltransferases found in most organisms [33, 34]. In spite of their highly conserved structure, sirtuins represent a variety of biological functions mainly due to their different enzymatic activities and binding partners [35]. Seven sirtuin homologs (Sirt1–7) have been identified with distinct tissue distributions and subcellular localisations [36]. SIRT1, SIRT6, and SIRT7 are nuclear residents, while SIRT2 has a cytosolic localisation and SIRT3, SIRT4, and SIRT5 are found in mitochondria [37]. SIRT3 has also a nuclear form [36].

Sirtuins are known to be involved in the physiology and pathophysiology of heart [38]. Mitochondrial proteins are one of the main targets of the sirtuin regulatory networks. Sirtuins modulate the mitochondrial function by reversible acetylation of the ε-amino group of internal lysine residues of mitochondrial proteins, a mechanism called acetylation [39]. The nuclear sirtuin, SIRT1 deacetylates and activates PGC1 alpha, a master metabolic coactivator in mitochondria regulating mitochondrial metabolism, biogenesis and respiration [40-43]. PGC1 alpha deacetylation enhances its activity to co-activate transcription factors including PPAR alpha [14]. This, in its turn, results in the transcription of target genes involved in fatty acid oxidation and oxidative phosphorylation [40, 44]. Inhibition of SIRT1 activity, depletion of SIRT1 or increased level of GCN5, an acetyltransferase which acetylates PGC-1 at several lysine residues, inhibits the PGC1 transcriptional activity in muscle and liver [45, 46]. In good agreement with these observations, we found increased levels of acetylated (inactive) PGC1 in irradiated male hearts suggesting impairment in the co-activator function of PGC1 after irradiation.

Among the mitochondrial sirtuins, SIRT3 is a major mitochondrial deacetylase. The full length SIRT3 is a 44 kD protein with an N-terminal mitochondrial targeting sequence that is proteolytically processed to a mature 28 kD catalytically active SIRT3 deacetylase [47-49] with a wide range of target proteins including those involved in mitochondrial respiration, electron transport chain, TCA cycle, and fatty acid oxidation as well as oxidative stress defence [38]. The activity of SIRT3 is tightly regulated by availability of its substrate, NAD+. It has been shown that the mitochondrial Complex I deficiency results in NADH accumulation and a reduction in the NAD+/NADH ratio inhibits SIRT3 activity. The reduced deacetylation activity of SIRT3 leads to the hyperacetylation of mitochondrial proteins and subsequently abnormalities in mitochondrial energy metabolism [48]. In this study, the immunoblotting analysis showed significant downregulation of mitochondrial SIRT3 in heart tissue in the high-dose groups of 100 - 500 mGy and > 500 mGy. The expression of two other mitochondrial sirtuins, SIRT4 and SIRT5, showed reduced expression only in the group > 500 mGy.

Alteration of mitochondrial oxidative phosphorylation has been reported to increase the reactive oxygen species (ROS) production [50]. We have shown previously that local heart irradiation permanently increases mitochondrial ROS levels in mice [23, 24]. In our previous study on cardiac tissue from Mayak workers, we showed a dose-dependent decrease in the level of the antioxidant response regulator protein NRF2 and its target genes [13]. The immunoblotting analysis showed here a significant decrease in the oxidative response enzymes, GSTK1 and CAT in irradiated hearts. However the expression level of NRF2 itself was not changed.

6 CONCLUSIONS

The present study confirmed the previous observations in the irradiated hearts of male Mayak workers. Data presented here suggest that chronic radiation exposure induces impairment of cardiac metabolism and thus accelerates the pathogenesis of ischemic heart disease. The metabolic disorder is associated with the impairment of SIRT / PGC1 / PPAR alpha activity (Figure 17). Understanding the mechanism of radiation-induced heart disease is necessary for constructing mathematical models of the damage process that are essential in extrapolating epidemiological data.

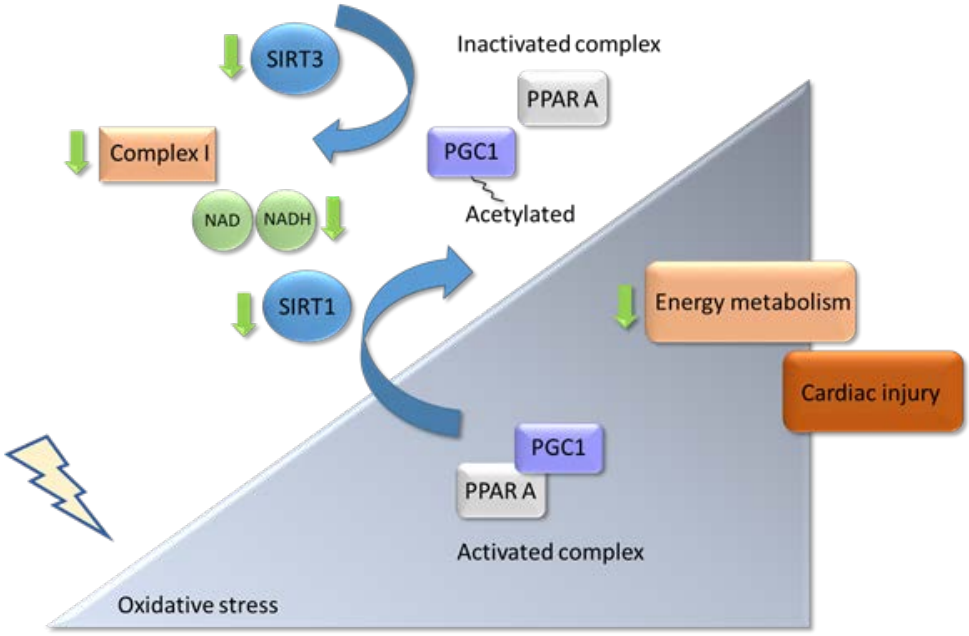

Figure 6-1 Disruption of SIRT / PGC1/ PPAR alpha regulatory network contributes in radiation-induced cardiac damage.

7 OUTLOOK

In most countries, the radiation risks for men and women have been averaged together for the routine regulatory purposes. However, these standards and recommendations apply only for low doses close to the background levels. Very little information about gender differences is available for exposure situations at moderate and high radiation doses exceeding 100 mGy, although it is this range of doses having a large negative health impact. In such instances it will be necessary to consider the gender, age, and other mitigating factors in making a risk assessment. This study indicates that similar biological pathways are involved in the cardiac response of men and women. However, the low sample number especially in the higher dose groups of the female workers makes it difficult to give a statistically significant statement about the similarities or differences in the radiation response between the genders. In particular, the question whether a possible threshold dose exists and, if yes, whether it is gender specific, remains unanswered. Therefore, it would be necessary to continue collecting and analysing this valuable material and thereby increase the knowledge of gender specificity of radiation-induced heart disease in human.

8 BIBLIOGRAPHY

1. Azizova, T.V., et al., *Ischaemic heart disease incidence and mortality in an extended cohort of Mayak workers first employed in 1948-1982.* Br J Radiol, 2015. **88**(1054): p. 20150169.
2. Azizova, T.V., et al., *Cardiovascular diseases in the cohort of workers first employed at Mayak PA in 1948-1958.* Radiat Res, 2010. **174**(2): p. 155-68.
3. Simonetto, C., et al., *Ischemic heart disease in workers at Mayak PA: latency of incidence risk after radiation exposure.* PLoS One, 2014. **9**(5): p. e96309.
4. Yamada, M., et al., *Noncancer disease incidence in atomic bomb survivors, 1958-1998.* Radiat Res, 2004. **161**(6): p. 622-32.
5. Stanley, W.C. and C.L. Hoppel, *Mitochondrial dysfunction in heart failure: potential for therapeutic interventions?* Cardiovasc Res, 2000. **45**(4): p. 805-6.
6. Walters, A.M., G.A. Porter, Jr., and P.S. Brookes, *Mitochondria as a drug target in ischemic heart disease and cardiomyopathy.* Circ Res, 2012. **111**(9): p. 1222-36.
7. Lehman, J.J. and D.P. Kelly, *Gene regulatory mechanisms governing energy metabolism during cardiac hypertrophic growth.* Heart Fail Rev, 2002. **7**(2): p. 175-85.
8. Fillmore, N., J. Mori, and G.D. Lopaschuk, *Mitochondrial fatty acid oxidation alterations in heart failure, ischaemic heart disease and diabetic cardiomyopathy.* Br J Pharmacol, 2014. **171**(8): p. 2080-90.
9. Barger, P.M. and D.P. Kelly, *PPAR signaling in the control of cardiac energy metabolism.* Trends Cardiovasc Med, 2000. **10**(6): p. 238-45.
10. Finck, B.N., *The PPAR regulatory system in cardiac physiology and disease.* Cardiovasc Res, 2007. **73**(2): p. 269-77.
11. Azimzadeh, O., et al., *PPAR Alpha: A Novel Radiation Target in Locally Exposed Mus musculus Heart Revealed by Quantitative Proteomics.* Journal of Proteome Research, 2013. **12**(6): p. 2700-2714.
12. Breckenridge, R., *Heart failure and mouse models.* Dis Model Mech, 2010. **3**(3-4): p. 138-43.
13. Azimzadeh, O., et al., *A dose-dependent perturbation in cardiac energy metabolism is linked to radiation-induced ischemic heart disease in Mayak nuclear workers.* Oncotarget, 2017. **8**(6): p. 9067-9078.
14. Anspaugh, L.R., M.O. Degteva, and E.K. Vasilenko, *Mayak Production Association: introduction.* Radiat Environ Biophys, 2002. **41**(1): p. 19-22.
15. Azimzadeh, O., et al., *Rapid proteomic remodeling of cardiac tissue caused by total body ionizing radiation.* Proteomics, 2011. **11**(16): p. 3299-311.
16. Wisniewski, J.R., et al., *Universal sample preparation method for proteome analysis.* Nat Methods, 2009. **6**(5): p. 359-62.
17. Hauck, S.M., et al., *Deciphering membrane-associated molecular processes in target tissue of autoimmune uveitis by label-free quantitative mass spectrometry.* Mol Cell Proteomics, 2010. **9**(10): p. 2292-305.
18. Wu, J., et al., *Comparative proteomic characterization of articular cartilage tissue from normal donors and patients with osteoarthritis.* Arthritis Rheum, 2007. **56**(11): p. 3675-84.
19. Barger, P.M., et al., *Deactivation of peroxisome proliferator-activated receptor-alpha during cardiac hypertrophic growth.* J Clin Invest, 2000. **105**(12): p. 1723-30.
20. Dorn, G.W., 2nd, R.B. Vega, and D.P. Kelly, *Mitochondrial biogenesis and dynamics in the developing and diseased heart.* Genes Dev, 2015. **29**(19): p. 1981-91.

21. Fan, W. and R. Evans, *PPARs and ERRs: molecular mediators of mitochondrial metabolism.* Curr Opin Cell Biol, 2015. **33**: p. 49-54.

22. Azimzadeh, O., et al., *Label-free protein profiling of formalin-fixed paraffin-embedded (FFPE) heart tissue reveals immediate mitochondrial impairment after ionising radiation.* J Proteomics, 2012. **75**(8): p. 2384-95.

23. Barjaktarovic, Z., et al., *Radiation-induced signaling results in mitochondrial impairment in mouse heart at 4 weeks after exposure to X-rays.* PLoS One, 2011. **6**(12): p. e27811.

24. Barjaktarovic, Z., et al., *Ionising radiation induces persistent alterations in the cardiac mitochondrial function of C57BL/6 mice 40 weeks after local heart exposure.* Radiother Oncol, 2013. **106**(3): p. 404-10.

25. Lesnefsky, E.J., et al., *Ischemia, rather than reperfusion, inhibits respiration through cytochrome oxidase in the isolated, perfused rabbit heart: role of cardiolipin.* Am J Physiol Heart Circ Physiol, 2004. **287**(1): p. H258-67.

26. Tompkins, A.J., et al., *Mitochondrial dysfunction in cardiac ischemia-reperfusion injury: ROS from complex I, without inhibition.* Biochim Biophys Acta, 2006. **1762**(2): p. 223-31.

27. Gregersen, N., J. Hansen, and J. Palmfeldt, *Mitochondrial proteomics--a tool for the study of metabolic disorders.* J Inherit Metab Dis, 2012. **35**(4): p. 715-26.

28. Shen, X., et al., *Quantitative proteomics in cardiovascular research: global and targeted strategies.* Proteomics Clin Appl, 2014. **8**(7-8): p. 488-505.

29. Karamanlidis, G., et al., *Mitochondrial complex I deficiency increases protein acetylation and accelerates heart failure.* Cell Metab, 2013. **18**(2): p. 239-50.

30. Srivastava, S., *Emerging therapeutic roles for NAD(+) metabolism in mitochondrial and age-related disorders.* Clin Transl Med, 2016. **5**(1): p. 25.

31. Watanabe, K., et al., *Constitutive regulation of cardiac fatty acid metabolism through peroxisome proliferator-activated receptor alpha associated with age-dependent cardiac toxicity.* J Biol Chem, 2000. **275**(29): p. 22293-9.

32. Finck, B.N., et al., *A critical role for PPARalpha-mediated lipotoxicity in the pathogenesis of diabetic cardiomyopathy: modulation by dietary fat content.* Proc Natl Acad Sci U S A, 2003. **100**(3): p. 1226-31.

33. Frye, R.A., *Phylogenetic classification of prokaryotic and eukaryotic Sir2-like proteins.* Biochem Biophys Res Commun, 2000. **273**(2): p. 793-8.

34. Saunders, L.R. and E. Verdin, *Sirtuins: critical regulators at the crossroads between cancer and aging.* Oncogene, 2007. **26**(37): p. 5489-504.

35. Haigis, M.C. and D.A. Sinclair, *Mammalian sirtuins: biological insights and disease relevance.* Annu Rev Pathol, 2010. **5**: p. 253-95.

36. Lavu, S., et al., *Sirtuins--novel therapeutic targets to treat age-associated diseases.* Nat Rev Drug Discov, 2008. **7**(10): p. 841-53.

37. Houtkooper, R.H., E. Pirinen, and J. Auwerx, *Sirtuins as regulators of metabolism and healthspan.* Nat Rev Mol Cell Biol, 2012. **13**(4): p. 225-238.

38. Matsushima, S. and J. Sadoshima, *The role of sirtuins in cardiac disease.* Am J Physiol Heart Circ Physiol, 2015. **309**(9): p. H1375-89.

39. Polevoda, B. and F. Sherman, *The diversity of acetylated proteins.* Genome Biol, 2002. **3**(5): p. reviews0006.

40. Jeninga, E.H., K. Schoonjans, and J. Auwerx, *Reversible acetylation of PGC-1: connecting energy sensors and effectors to guarantee metabolic flexibility.* Oncogene, 2010. **29**(33): p. 4617-24.

41. Lin, Z. and D. Fang, *The Roles of SIRT1 in Cancer.* Genes Cancer, 2013. **4**(3-4): p. 97-104.

42. Kelly, D.P., *The pleiotropic nature of the vascular PPAR gene regulatory pathway.* Circ Res, 2001. **89**(11): p. 935-7.

43. Park, D.R., J.S. Kim, and C.K. Kim, *The effect of SIRT1 protein knock down on PGC-1alpha acetylation during skeletal muscle contraction.* J Exerc Nutrition Biochem, 2014. **18**(1): p. 1-7.

44. Verdin, E., et al., *Sirtuin regulation of mitochondria: energy production, apoptosis, and signaling.* Trends Biochem Sci, 2010. **35**(12): p. 669-75.

45. Purushotham, A., et al., *Hepatocyte-specific deletion of SIRT1 alters fatty acid metabolism and results in hepatic steatosis and inflammation.* Cell Metab, 2009. **9**(4): p. 327-38.

46. Moreno, M., et al., *PPARs: Nuclear Receptors Controlled by, and Controlling, Nutrient Handling through Nuclear and Cytosolic Signaling.* PPAR Res, 2010. **2010**.

47. Onyango, P., et al., *SIRT3, a human SIR2 homologue, is an NAD-dependent deacetylase localized to mitochondria.* Proc Natl Acad Sci U S A, 2002. **99**(21): p. 13653-8.

48. Lombard, D.B., et al., *Mammalian Sir2 homolog SIRT3 regulates global mitochondrial lysine acetylation.* Mol Cell Biol, 2007. **27**(24): p. 8807-14.

49. Schwer, B., et al., *The human silent information regulator (Sir)2 homologue hSIRT3 is a mitochondrial nicotinamide adenine dinucleotide-dependent deacetylase.* J Cell Biol, 2002. **158**(4): p. 647-57.

50. Heather, L.C., et al., *Critical role of complex III in the early metabolic changes following myocardial infarction.* Cardiovasc Res, 2010. **85**(1): p. 127-36.

LIST OF FIGURES

LIST OF TABLES

LIST OF ABBREVIATIONS

A-bomb	Atomic bomb
ACAT	Acetyl-CoA acetyltransferase
ACN	Acetonitrile
AmBic	Ammonium bicarbonate
ANOVA	Analysis of variance
ATP	Adenosine triphosphate
BMI	Body mass index
BSA	Bovine serum albumin
CAT	Catalase
CeVD	Cerebrovascular disease
CPT	Carnitine O-palmitoyltransferase
DTT	Dithiothreitol
ECL	Electrochemiluminescence
EIF2	Eukaryotic initiation factor 2
ESI	Electrospray ionization
FASP	Filter-aided sample preparation
GSTK1	Glutathione S-transferase kappa 1
Gy	Gray
HADHA	Long-chain (S)-3-hydroxyacyl-CoA
HCM	Human cardiac myocytes
HMGU	Helmholtz Zentrum München
HPLC	High performance liquid chromatography
IAA	Iodoacetamide
ICD-9	International Statistical Classification of Diseases and Related Health Problems, version 9
ID	Identifier
IgG	Immunoglobulin G
IHD	Ischemic heart disease
IPA	Ingenuity pathway analysis
ISB	Institute of Radiation Biology, Helmholtz Zentrum München
kBq	Kilobequerel
kDa	Kilodalton
LC	Liquid chromatography
MS/MS	Tandem mass spectrometry
NAD	Nicotinamide adenine dinucleotide
NADH	Reduced NAD
NRF-2	Nuclear factor (erythroid-derived 2)-like 2
OXPHOS	Oxidative phosphorylation
PA	Production Association
PGC1	Peroxisome proliferator-activated receptor gamma coactivator 1
PPAR alpha	Peroxisome proliferator-activated receptor alpha
RXR	Retinoid X receptor
SDS-PAGE	Sodium dodecyl sulfate polyacrylamide gel electrophoresis
SEM	Standard error of the mean
SIRT	Sirtuin
SUBI	Southern Urals Biophysics Institute
TCA	Tricarboxylic acid
TBS	Tris-buffered saline

TFA	Trifluoroacetic acid
TCA	Tricarboxylic acid
Tris/HCl	Tris(hydroxymethyl)aminomethane/Hydrochloric acid
UA	Uric acid
WST-1	Stable tetrazolium salt

| Verantwortung für Mensch und Umwelt |

Kontakt:
Bundesamt für Strahlenschutz
Postfach 10 01 49
38201 Salzgitter
Telefon: + 49 30 18333 – 0
Telefax: + 49 30 18333 – 1885
Internet: www.bfs.de
E-Mail: ePost@bfs.de
Gedruckt auf Recyclingpapier aus 100 % Altpapier.

Bundesamt für Strahlenschutz